Automotive Application of Multi-Phase Coupled-Inductor DC-DC Converter

J. Czogalla
Jieli Li
C. R. Sullivan

Found in *IEEE Industry Applications Society Annual Meeting,* Oct. 2003, pp. .

Automotive Application of Multi-Phase Coupled-Inductor DC-DC Converter

Jens Czogalla, Jieli Li*, and Charles R. Sullivan
Thayer School of Engineering, Dartmouth College
http://engineering.dartmouth.edu/inductor charles.r.sullivan@dartmouth.edu
8000 Cummings Hall, Hanover, NH 03755, USA, Tel. +1-603-646-2851 Fax +1-603-646-3856
*Volterra Semiconductor Corp., Fremont CA USA

***Abstract*— A set of four coupled inductors is applied to a four-phase interleaved 1 kW bi-directional 14 V to 42 V dc/dc converter for automotive applications. The coupled-inductor structure is optimized, and the performance is examined through simulations and experimental measurements. Although coupled inductors offer bigger advantages in applications that require fast transient response, they also have significant advantages in this type of application.**

I. Introduction

Buck converters comprising several parallel sections, operated staggered in phase (interleaved) have become popular, particularly for microprocessor power delivery circuits (often referred to as VRMs—voltage regulator modules). Recent work has shown that introducing coupling between the inductors in the different phases of such a multi-phase converter can offer dramatic advantages for microprocessor power delivery applications, because it can offer very fast transient response without large inductor-current ripple [1], [2]. In this paper, we examine the advantages that coupled inductors can offer for an application in which transient response is not an important consideration: an automotive 14 V to 42 V bi-directional dc-to-dc converter.

Low-cost, but efficient and reliable 14 V to 42 V bidirectional dc-to-dc converters will soon be in great demand. For the year 2005, reference [3] expects the electrical power needed in a car to be between 3000 W and 7000 W [3]. This electrical power demand can not be handled by the 14 V electrical system. To solve this problem a new 42 V standard has been developed [4].

Before the transition to the 42 V system is completed, many vehicles will require both 42 V and 14 V buses to accommodate the electrical subsystems still working with 14 V [5]. One possible architecture for such a dual voltage electrical system includes A 36 V battery is connected to the 42 V bus and a 12 V battery is connected to the 14 V bus. The generator supplies the 42 V bus, and a bi-directional dc/dc converter is required to charge the 12 V battery or to supply power from the 12 V battery to the 42 V bus [5].

This work was supported in part by the United States Department of Energy under grant DE-FC36-01GO1106

In power converters for microprocessor power delivery, fast response to transients is essential. Small inductor values can help, but that approach leads to large ripple currents and thus high losses. Using coupled inductors can help the designer bypass this tradeoff. In [6], [7] it was shown that coupling the inductors in a two-phase interleaved converter can effect a reduction in ripple. A topology using three gaped legs was introduced. Based on this work, [1], [2] show a different gapping configuration for two-phase converters which leads to higher ripple reduction. Additionally, a topology that allows practical operation with strong coupling and with more than two phases was introduced. The result was significant performance improvements; the ripple current in the inductors and the MOSFETs could be reduced without degrading the transient response time [1], [2].

In our automotive application, however, transient response is not important — batteries are available on both sides of the converter to buffer transients. The most important considerations are simply cost, efficiency and size. In the work presented here, we have found that coupled inductors offer significant advantages even when transient response is not a consideration.

II. Principle Of Operation

For the purpose of explaining the basic principle of coupled inductors, we discuss only a two-phase system in this section. In Section III, a model of a multiphase coupled-inductor converter will be presented.

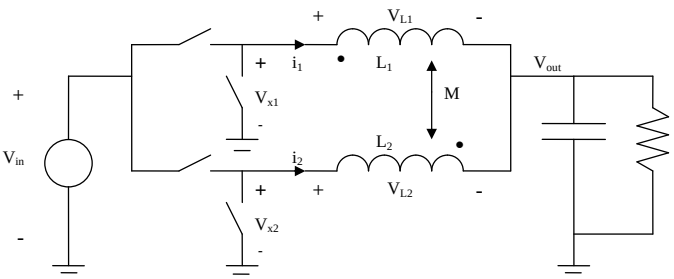

Fig. 1. 2-phase buck converter with coupled inductors.

The basic topology of a two-phased coupled inductor is shown in Fig. 1. The two phase inductors L_1 and L_2 are coupled together and the mutual inductance M represents the coupling effect between the two inductors. The dots, placed as shown in Fig. 1, indicate a negative value of M for the voltage polarities shown. The voltages applied across the two corresponding windings are related to the currents by [6]:

$$v_{L1} = L_1 \frac{di_1}{dt} + M \frac{di_2}{dt} \tag{1}$$

$$v_{L2} = L_2 \frac{di_2}{dt} + M \frac{di_1}{dt} \tag{2}$$

One can see that the current slope of one inductor is affected by the voltage across the other inductor; as shown in [6], [7], [1], [2], the result is reduced ripple current.

If we wish to consider the coupling factor

$$\alpha = \frac{M}{L} \tag{3}$$

and analyze its effect on the ripple, it is important to first consider which other parameter(s) will be held fixed. In [7], [1], [2], the leakage inductance is held constant in order to keep the transient response constant, and it is shown that increasing α as high as possible minimizes ripple. For our application, transient response is not important; we wish to minimize the size and cost of the converter without degrading efficiency. As a first approximation, the energy storage can be used as a proxy for the size and cost of a magnetic component. Holding leakage inductance constant also means that the energy storage is fixed, and so is an appropriate condition for comparing different degrees of coupling, even when transient response is not a primary concern.

The ratio of ripple with coupling to the ripple without coupling, based on holding the leakage inductances, and thus the energy storage, fixed is given by [6]

$$\frac{\Delta i_{L,coup}}{\Delta i_{L,uncoup}} = \frac{1 + \alpha \frac{D}{1-D}}{1 - \alpha}. \tag{4}$$

Note that α is between -1 and 0 because M is negative.

Uncoupled inductors correspond to $\alpha = 0$. The coupling effect gets stronger as the absolute value of α increases, and thus the current ripple is reduced. The smallest ripple can be achieved when there is perfect coupling (α = -1). In practice perfect coupling can not be realized, but the highest practical value of α gives the best ripple reduction.

The operation of the coupled-inductor converter may also be understood in terms of a transformer model including leakage inductance and magnetizing inductance, as described in [1]. Although the terminal behavior of the transformer model is identical to the behavior described by (1) and (1), it offers a different way of thinking about the circuit operation that may be more intuitive. The interested reader is referred to [1].

To use the advantages of coupled inductors in a converter with any number of phases, [1], [2] introduced a "ladder core" inductor topology. This topology affords strong coupling for multi-phase inductors, which cannot be achieved with other topologies, as confirmed by the review of possible multi-phase coupling topologies in [8].

III. Design

A. Model Formulation

One way to construct the the ladder core topology for multi-phase coupling [1] using only standard core shapes is shown in Fig. 2 [2].

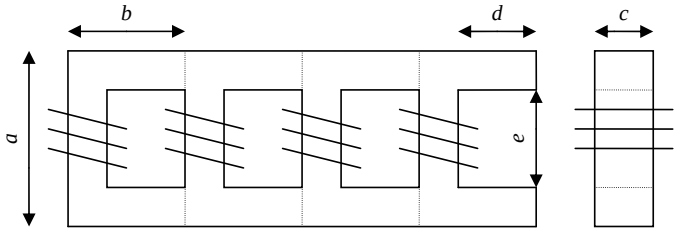

Fig. 2. Core configuration used, shown for four phases.

In [1] the magnetic circuit shown in Fig. 3 is developed to analyze the behavior of the ladder core structure. In Fig. 3, $\mathcal{R}_l$ is the leakage reluctance, $\mathcal{R}_{tb}$ is the sum of the reluctances of top and bottom outer legs across any one window, and $\mathcal{R}_u$ is the reluctance of the rung of the ladder, which is also the post around which the wire is wound. Each MMF source corresponds to a winding, with a value Ni equal to the product of the the current i and number of turns N in the corresponding winding [1].

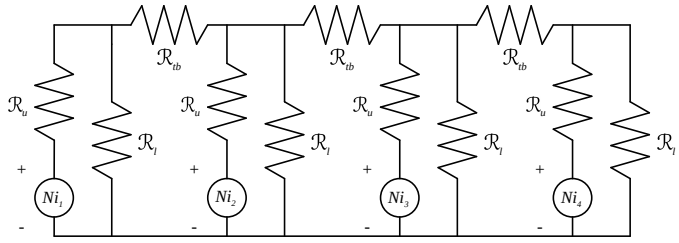

Fig. 3. Magnetic circuit model for four-phase coupled inductor. From [1].

Based on Fig. 3 [1] writes

$$\Phi_u = \mathbf{A}\mathcal{F}, \tag{5}$$

where Φ_u is a vector containing the magnetic flux in each rung of the ladder structure, $\mathcal{F}$ is a vector of the MMF values at each node at the top of Fig. 3, and, for four phases,

$$\mathbf{A} = \begin{bmatrix} \frac{1}{\mathcal{R}_{tb}} + \frac{1}{\mathcal{R}_\ell} & -\frac{1}{\mathcal{R}_{tb}} & 0 & 0 \\ -\frac{1}{\mathcal{R}_{tb}} & \frac{2}{\mathcal{R}_{tb}} + \frac{1}{\mathcal{R}_\ell} & -\frac{1}{\mathcal{R}_{tb}} & 0 \\ 0 & -\frac{1}{\mathcal{R}_{tb}} & \frac{2}{\mathcal{R}_{tb}} + \frac{1}{\mathcal{R}_\ell} & -\frac{1}{\mathcal{R}_{tb}} \\ 0 & 0 & -\frac{1}{\mathcal{R}_{tb}} & \frac{1}{\mathcal{R}_{tb}} + \frac{1}{\mathcal{R}_\ell} \end{bmatrix}, \tag{6}$$

The matrix $\mathbf{A}$ may be similarly expressed for any number of phases. From

$$\Phi_u = \frac{Ni - \mathcal{F}}{\mathcal{R}_u}, \tag{7}$$

an expression for the vector of currents in each winding as a function of the vector of flux in each rung can be found. [1]

$$i = \frac{1}{N}(\mathcal{R}_u + A^{-1})\Phi_u \tag{8}$$

B. Calculation of Steady State Waveforms

The magnetic flux waveforms and current waveforms are calculated using the model derived above as described in [1]. Both waveforms have dc components and ac components which are calculated separately.

The dc components are calculated by assuming that the dc currents in each phase are equal [1]. This is necessary for proper operation, and may be achieved by the same active or passive methods that are used for uncoupled multi-phase converters. Thus, with total current in the load I_{total} and n phases, the dc component of current in each phase is $I_{phase,dc} = I_{total}/n$. The dc component of flux in the outside legs of the ladder core (top and bottom in Fig. 2) is zero and the flux in each rung is [1]

$$\Phi_{u,dc} = \frac{NI_{phase,dc}}{\mathcal{R}_u + \mathcal{R}_\ell}. \tag{9}$$

The voltage across each winding will switch from $V_{in} - V_{out}$ to $-V_{out}$. The relationship between the flux change in the rung and the voltage is [1]

$$V = -N\frac{d\Phi_u}{dt} \tag{10}$$

From the duty cycle and the period, (10) can be used to obtain the ac component of flux in the rung, and from equation (8), the ac components the winding currents can be calculated [1]. The ac component of the MMF $\mathcal{F}$ can be found by inverting (5); the MMF can then be used to calculate flux in the outside legs of the ladder core (top and bottom in Fig. 2) using [1]

$$\Phi_{tb} = \frac{\Delta\mathcal{F}}{\mathcal{R}_{tb}}. \tag{11}$$

Now we have all the components of fluxes and currents. Example waveforms are shown in Fig. 4, for the first four-phase coupled-inductor converter described in Section V with inductors wound with eight turns on a single set of U cores..

C. Calculation of Power Loss

We are taking three components of power loss into account. These are winding loss, magnetic core loss, and the losses in the circuit.

The winding loss is calculated as [9]:

$$P_{winding} = I_{dc}^2 R_{dc} + I_{ac,rms}^2 R_{ac} \tag{12}$$

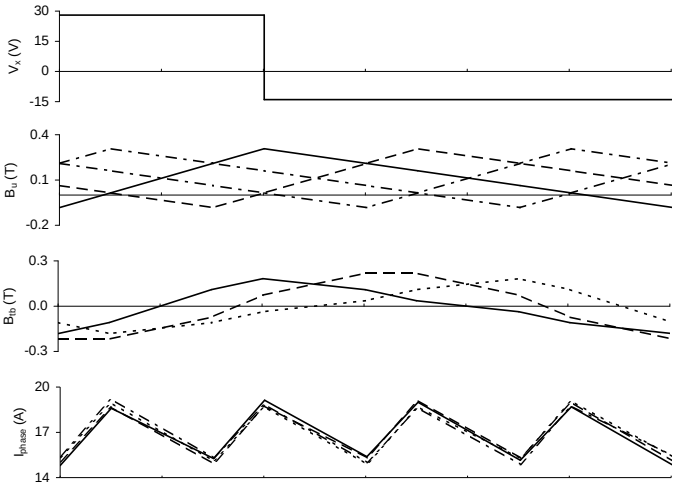

Fig. 4. Example waveforms calculated as described in the text for the first four-phase coupled-inductor converter described in Section V with inductors wound with eight turns on a single set of U cores. Shown for each phase are: The first switching-node voltages v_{x1}, all four outer core leg flux densities B_{tb}, all four core rung flux densities B_u, and all four phase currents i.

With high-frequency current, winding loss increases because of eddy-current effects [10]. As described above, we can achieve small ripple current with strong coupling, which means that the eddy-current effects do not influence the winding losses very strongly. Thus a simple approximation for R_{ac} in a single-layer winding is adequate:

$$R_{ac} = \frac{\pi d}{4\delta} R_{dc} \tag{13}$$

where d is the wire diameter and δ is the skin depth. We assume that AC current flows only within a small part of the cross section of the wire and not on surfaces facing a high-permeability core. The size of this area is determined by the skin depth which depends on the frequency of the AC current. Note that although (13) is only a rough approximation, more commonly used ac resistance formulas can have very large error [11].

For calculating core loss in ferrites, the Steinmetz equation is commonly used [12]:

$$P_v = k f^\alpha \hat{B}^\beta \tag{14}$$

where k, α, β are constants given by the manufacturer of the magnetic material, P_v is power loss per unit volume, $\hat{B}$ is peak flux density, and f is the frequency of sinusoidal excitation. The Steinmetz equation in this form can only be used for sinusoidal waveforms. To solve this problem, we use the "improved Generalized Steinmetz Equation" (iGSE) introduced in [12] for analyzing for losses with arbitrary nonsinusoidal waveforms. In reference [12] the effectiveness of the iGSE was experimentally verified.

Besides the losses in the inductor, we consider the losses in the circuit. We assume that the ripple reduction reduces

TABLE I
PARAMETERS FOR OPTIMIZATION

Symbol		Value
V_{in}	Input voltage	42 V
V_{out}	Output voltage	14 V
I_{total}	Total output current	68 A
$L_{l,tot}$	Parallel combination of leakage inductances	478 nH
n	Number of phases	4
E_{switch}	Total switching loss per cycle for all phases	13.38 μJ
R_{low}	On-resistance of low-side switches	8.7 mΩ
R_{high}	On-resistance of high-side switches	8.7 mΩ
d_{AWG}	AWG number of the wire used	16
	Geometrical parameters as defined in Fig. 2	
	a = 25 mm, b = 16 mm, c = 12 mm d = 10 mm, e = 13 mm	
	Parameters for core material: 3F3	MKS units
k	Core loss constant for (14)	$1.895{\cdot}10^{-5}$
α	Core loss frequency exponent	1.8
β	Core loss flux density exponent	2.5
k_1	Core loss constant	$2.5{\cdot}10^{-6}$
μ_r	Relative permeability of core material	2000

the losses in the output-capacitor to near zero [1]. So we do not take these losses into account, and analyze only the losses in the MOSFET switches. We can make the standard assumption (e.g., see [13]) that the total loss per switching cycle is fixed [9]. We represent this as E_{switch}, including gate drive loss. Multiplication by the switching frequency yields the switching power loss.

The combination of the on-resistances of both switches of each phase is given by [1]:

$$R_{on,eff} = DR_{high-side} + (1-D)R_{low-side} \qquad (15)$$

where $R_{high-side}$ and $R_{low-side}$ are the resistances of the high-side and low-side switches and D is the duty-cycle of the high-side switch. Multiplication of the square of the rms current by (15) yields the conduction loss [1].

Table I shows the values of E_{switch}, R_{low}, and R_{high} which were used for the optimization in Section IV. The values are based the datasheet of the commercial MOSFET SUP75N08-10.

IV. OPTIMIZATION

The calculation of losses in Section III is used to optimize the design of the coupled inductors. As in in [1], a standard numerical optimization algorithm — the Nelder-Mead simplex algorithm as implemented in the MATLAB function `fminsearch` [14] — was used to minimize loss.

In [1] numerous free parameters were used. In our first optimization, we have only three free parameters: the number of winding turns, the switching frequency, and the leakage inductance. The optimization starts with a bi-directional one kilowatt converter that was optimized with uncoupled inductors in [15]. Originally the converter operated with five uncoupled phases, but it was modified to work with four phases. Table I shows the fixed parameters based on this converter. The inductor design is based on the configuration shown in Fig. 2, but using a pair of stacked U cores, each with a dimension c of 6 mm.

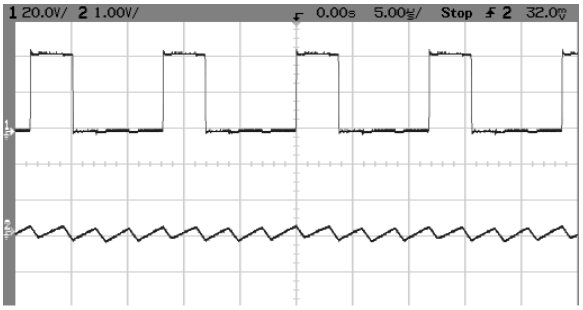

Fig. 5. Waveforms with good coupling. The upper waveform shows the rectangular waveform produced by the switch (20 V/div). The lower waveform shows the ac component of inductor current (10 A/div). The time scale is 5 μs/div.

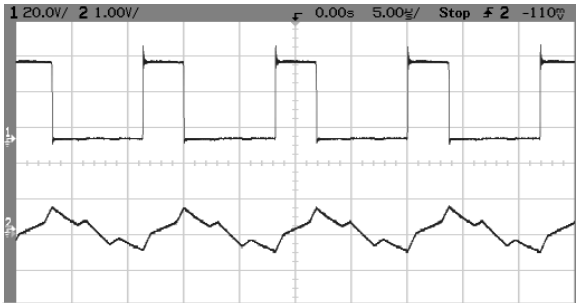

Fig. 6. Waveforms with poor coupling. The upper waveform shows the rectangular waveform produced by the switch (20 V/div). The lower waveform shows the ac component of inductor current (10 A/div). The time scale is 5 μs/div.

Table II summarizes the design details and performance for different numbers of winding turns. We see that the best results are for numbers of turns between five and seven, with per-phase switching frequencies between 73 and 47 kHz. Although frequencies for non-optimal numbers of turns range widely, the frequencies for the best turn numbers are close to the original switching frequency of 82 kHz, which is not surprising given the careful optimization that was performed on the original design [15].

If we do not limit the design to using standard core shapes, but rather assume that a custom core shape would be developed for high-volume production of coupled-inductor converters, significant improvements are possible. Table III shows that the design with an optimized core, using the same core volume as the original uncoupled inductors, is predicted to achieve a 0.7 W reduction in loss relative to the coupled design built on a standard core. This is still with a rectangular core; a round center-post core would allow further improvements.

TABLE II
OPTIMIZATION RESULTS FOR 68 A 42 V TO 14 V CONVERTER

N	Number of turns	3	4	5	6	7	8	9	
f_s	switching frequency (per phase)	147.5	98.3	72.6	57.8	47.0	40.9	35.9	kHz
$L_{l,tot}$	Parallel combination of all leakage inductances	1010	1247	1472	1705	1906	2163	2404	nH
I_{rms}	Total rms current	17.01	17.01	17.01	17.01	17.01	17.01	17.01	A
$I_{p,p}$	Peak-to-peak ripple current	2.21	2.24	2.28	2.28	2.35	2.28	2.26	A
P_w	Winding loss	0.34	0.60	0.95	1.37	1.81	2.39	3.0	W
P_c	Core loss	2.72	1.77	1.26	0.94	0.74	0.58	0.48	W
P_s	MOSFET Switching loss	1.97	1.32	0.97	0.77	0.63	0.55	0.48	W
P_{rds}	MOSFET conduction loss	10.06	10.06	10.07	10.07	10.07	10.07	10.07	W
P_M	Total MOSFET loss	12.04	11.38	11.04	10.84	10.70	10.61	10.55	W
P_t	Total loss	15.10	13.76	13.25	13.15	13.24	13.60	14.02	W

TABLE III
RESULTS FOR OPTIMIZATION OF COUPLED INDUCTOR DESIGN WITH OPTIMIZED CORE SHAPE, BASED ON A 42 V TO 14 V 1 KW CONVERTER.

N	6	turns
f_s	44.1	kHz
$L_{l,total}$	1752	nH
a	28.14	mm
b	19.08	mm
c	13.81	mm
d	10.87	mm
e	17.73	mm
I_{rms}	17.01	A
$I_{p,p}$	2.85	A
$P_{winding}$	1.01	W
P_{core}	0.79	W
$P_{switching}$	0.59	W
P_{cond}	10.07	W
P_{MOSFET}	10.66	W
P_{total}	12.46	W

V. EXPERIMENTAL RESULTS

Our first prototype of the coupled inductors was built with eight winding turns on a set of four single cores, rather than the stacked cores described in the previous section. The measured parallel combination of all leakage inductances was 483 nH. Fig. 5 shows the current waveforms of the modified converter. They match the calculated waveforms of Fig. 4 very well. But one can see that, as mentioned in Section II, perfect coupling is not achievable. Fig. 6 shows an example of weaker coupling. The waveforms were taken from an early variant of the coupled inductors. Dirt between the contact surfaces of the U-cores created air gaps between them and impaired the coupling. After we cleaned the area of contact the coupling improved tremendously as shown in Fig. 5.

To evaluate the performance of the coupled-inductor designs, we constructed a design similar to one of the optimized designs in Table II. Because the five-turn design was close to the original switching frequency, we opted to use five turns with the original 82 kHz switching frequency. The inductors were hand-wound with multiple parallel layers of AWG #18 wire. The measured DC resistance of 1.05 mΩ was 8% higher than the predicted resistance due to imperfections in the hand-winding process.

The initial leakage inductance of 213 nH was lower than the desired value of 1586 nH. This is calculated to result in a power loss increase of 0.57 W compared the the predicted loss with the desired 1586 nH. An additional ferrite leakage path was added as shown in Fig. 7 to boost leakage inductance to 300 nH, with brings the predicted loss to within 0.3 W of the predicted loss with the desired 1586 nH. Better methods to increase leakage inductance are an important topic for future study and optimization work.

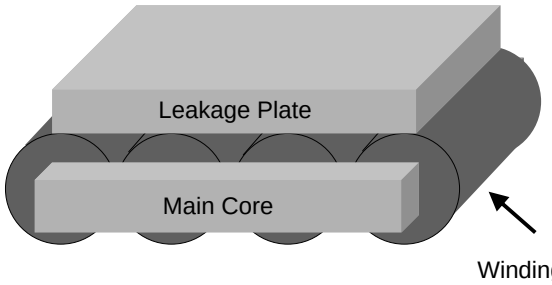

Fig. 7. Configuration of coupled inductors with additional ferrite plate placed on top to boost leakage inductance to 300 nH total parallel leakage inductance.

Fig. 8 shows the power loss of the coupled-inductor converter compared to that of the same four-phase converter operating with the original uncoupled inductors. Results from both the original coupled structure in Fig. 2 and the configuration with boosted leakage inductance shown in Fig. 7 are shown. The coupled designs have similar but slightly higher losses than the original design. This is achieved with smaller cores: four cores with 8620 mm^3 of ferrite each, compared to the inductors used in the uncoupled design which use RM10 cores with a volume of 1620 mm^3 each[1]. Thus we achieve similar performance with only 60 % of the original core material. With better winding construction, we expect that the coupled design could perform better than the uncoupled design. The design using the optimized core shapes shown in Table III should offer an even larger advantage relative to the uncoupled design.

[1]The original design used with eight turns of 33 twisted strands of AWG #30 copper wire on an RM10 core of Ferroxcube 3F3 material.

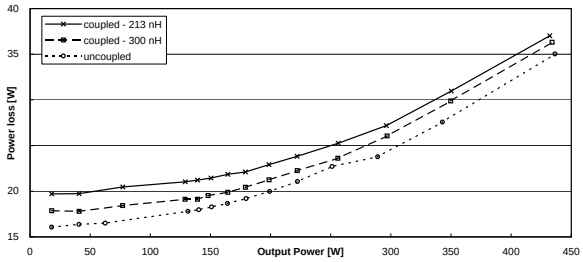

Fig. 8. Power loss of the converter using a four-phase coupled inductor compared to that of converter using uncoupled inductors. The converter is operated in buck mode, converting 42 v to 14 V

VI. Conclusion

Coupled inductors are known to offer advantages in applications requiring fast response — they allow reducing ripple current while keeping the leakage inductance, which determines transient response, constant. In applications where transient response is not important, low leakage inductance is also advantageous, because it corresponds to low energy storage, and thus smaller less expensive inductors. We have experimentally demonstrated good performance with coupled inductors in an automotive multi-phase dc-dc converter, using coupled inductors wound on standard core shapes using a smaller volume of magnetic material. Improved performance would be possible with better winding construction and/or custom designed cores.

Acknowlegement

Thanks to A. Pfaelzer and M. Weiner of Intronics Corp., Norwood, MA, for providing the converter we worked with.

References

[1] Jieli Li, Charles R. Sullivan, and Aaron Schultz, "Coupled inductor design optimization for fast-response low-voltage DC-DC converters", in *IEEE Applied Power Electronics Conference*, 2002.

[2] A. M. Schultz and C.R. Sullivan, "Voltage converter with coupled inductive windings, and associated methods", 2002, U.S. Patent number 6,362,986, Volterra Semiconductor Corp.

[3] Dr. Alfons Graf, Dieter Vogel, Josef Gantioler, and Dr. Frank Klotz, "Intelligent power semiconductors for future automotive electrical systems.", in *17. Meeting 'Elektronik im Kraftfahrzeug'*, June 1997.

[4] Paul Nicastri, "Jump starting and charging batteries with the new 42 v PowerNet", in *1st International Congress on 42VPowerNet*, August 1999.

[5] Norman Traub, "Dual/higher voltage — a global opportunity", in *Intertch 42-Volt Automotive System Summit*, 2001.

[6] Pit-Leong Wong, Q. Wu, Peng Xu, Bo Yang, and F.C. Lee, "Investigating coupling inductors in the interleaving QSW VRM", in *Proceedings of APEC 2000 - Applied Power Electronics Conf.*, 2000, vol. 2, pp. 973–978.

[7] Pit-Leong Wong, Peng Xu, P. Yang, and F.C. Lee, "Performance improvements of interleaving VRMs with coupling inductors", *IEEE Trans. on Power Electronics*, vol. 16, no. 4, pp. 499507, 2001.

[8] P. Zumel, O. Garca, J. Cobos, and J. Uceda, "Magnetic integration for interleaved converters", in *IEEE Applied Power Electronics Conference*, 2002.

[9] Jieli Li, "Coupled inductor design in dc-dc converters", Master's thesis, Thayer School of Engineering, Dartmouth College, December 2001.

[10] E. C. Snelling, *Soft Ferrites, Properties and Applications*, Butterworths, second edition, 1988.

[11] Xi Nan and C.R. Sullivan, "An improved calculation of proximity-effect loss in high frequency windings of round conductors", in *34th Annual IEEE Power Electronics Specialists Conference*, 2003.

[12] Jieli Li, T. Abdallah, and Charles R. Sullivan, "Improved calculation of core loss with nonsinusoidal waveforms", in *IEEE Industry Applications Society Annual Meeting*, Oct. 2001, p. 22032210.

[13] Robert W. Erickson, *Fundamentals of Power Electronics*, Kluwer Academic Publishers, fourth printing edition, 1999.

[14] J.C. Lagarias, J.A. Reeds, M.H. Wright, and P.E. Wright, "Convergence properties of the Nelder-Mead simplex method in low dimensions", *SIAM Journal on Optimization*, vol. 9, no. 1, pp. 112147, 1998.

[15] T.C. Neugebauer and D.J. Perreault, "Computer-aided optimization of dc/dc converters for automotive applications", *IEEE Transactions on Power Electronics*, vol. 18, no. 3, pp. 775 –783, May 2003.